

Coupled Numerical Simulation of an Aluminum and a Composite Hydrofoil in Steady Flows

Laetitia Pernod^{1,3}, Antoine Ducoin¹, Hervé Le Sourné², Jean-François Sigrist³

¹LHEEA laboratory, Ecole Centrale de Nantes (CNRS UMR 6598), Nantes, France

²GeM Institute (CNRS UMR 6183), ICAM Nantes, Carquefou, France

³DCNS Research, CESMAN, Technocampus Océan, 5 Rue de l'Halbrane, 44340 Bouguenais, France

ABSTRACT

The objective of this paper is to investigate the fluid structure interaction of a 3D NACA0009 composite hydrofoil in steady flows. The hydrofoil set up, which was originally developed experimentally by the Australian Maritime College (AMC), is clamped at the root and free at the tip section, and was designed to behave like a marine propeller blade (Zarruk et. al, 2014). 3D fluid structure computations are performed using a coupling between CFD (Computational Fluid Dynamic) and CSD (Computational Solid Dynamic) softwares, through tightly coupled algorithm. The hydrodynamic performances, structure natural frequencies and tip displacements are validated against experiments. Then the hydroelastic response is investigated. The results will help for the validation of a tightly coupled procedure, which will be used for the development and the optimization of a newly developed design of composite marine propeller.

Keywords

Composite hydrofoil, fluid-structure interaction, commercial software, numerical simulation, experimental validation

1 INTRODUCTION

The development of composite marine propellers for surface ship and submarines has been the subject of increasing researches in the last decade. Within the main objective of CO emissions reduction, the key design clearly remains in the development of lighter structures, but also in the modification of the structural properties to increase the propeller performances and to reduce the possible vibrations caused by the flow. Academic studies demonstrated that using a passive control of composite propellers thanks to their structural properties can successfully lead to performance improvements and reduced vibrations (Plucinski et. al, 2007), (He et. al, 2012). As a consequence, there is now a growing interest for Navies and shipyards to develop full scale prototypes (Yamatogi et. al, 2009).

It was shown that using composite materials instead of the usual metal alloys for marine propellers would be a

suitable solution to face the challenge. The passive control of deformations typically allows to reduce cavitation (Chen et. al, 2006, Young 2009), and it was also shown that the use of composites can lead to better hydrodynamic performances compared to conventional marine propellers due the bend-twist coupling property. Indeed, this bend-twist coupling enables the propeller to passively adapt to the incoming flow, and thus to increase performances for a wider range of ship speed (Plusincki et. al, 2007). (He et. al, 2012) were then successful in reducing the level of vibrations transmitted to the propeller shaft.

To achieve better performances, it becomes necessary to focus on the design and optimization of such self-adaptable propellers. (Lee and Lin, 2004) established the influence of the layers stacking sequence on the hydroelastic performances of composite propellers, and computed the optimal arrangement of the fibers using a genetic algorithm. (Liu and Young, 2007) also related the layers stacking sequence with the capacity of the composite propeller to passively adapt to the flow. In 2009, Liu and Young performed a systematic design method for composite propellers. A year after, (Blasques et. al, 2010) realized the optimization of a full-scale prototype and included the structural resistance as a criterion. More recently, (Lee et. al, 2015) optimized the stacking sequence for the investigation of the hydroelastic behavior of the propeller. That same year, (Garg et al, 2015) realized a hydrodynamic shape optimization of an unswept, tapered, cantilevered, aluminum alloy 3D hydrofoil developed and tested earlier by (Zarruk et al, 2014), (Cohen et. al, 2014) and (Philipps et. Al, 2015). (Garg et al, 2015) used a gradient-based optimizer associated with an adjoint method to carry out the optimization. This allowed them to consider a high number of design variables and to highlight their influence on the optimization. A cavitation constraint was also introduced in the optimization. In (Garg et al, 2017), the authors carried out a multipoint optimization on the same 3D hydrofoil, based on their previous developments. The experimental data from (Zarruk et al, 2014), (Cohen et. al, 2014) and (Philipps et. Al, 2015) is also used in this

study as a reference, and details from their work are presented later in this paper.

With the recent development and validation of effective fluid-structure methods, it is now possible to perform coupled CFD-CSD computations to validate a composite propeller, possibly designed using an optimization process, with consideration for the composite and plies layup and the geometry of the propeller. Structural resistance, cavitation and hydroelastic instabilities can be assessed using common staggered procedures between the codes (Young et al, 2016).

This work is the first step of validation of fluid-structure computations which will help the design of composite marine propellers. First, the hydrofoil properties are presented. Then, the governing equations used for the fluid and the structure are given, followed by the numerical models and the set-up used in simulations. The results show the validation against experiments, and then the hydroelastic response is investigated.

2 EXPERIMENTAL MODEL

The numerical model is taken from the experiments realized by Zarruk et. al in 2014, consisting of a composite and an isotropic hydrofoils tested under the same range of operating conditions in a water tunnel. The hydrofoils are cantilevered at the root and has a free tip that allows the structure to behave like a propeller blade. Details of the dimensions, manufacture, material and structural properties of the hydrofoils, as well as the experimental setup and instrumentation, can be found in (Zarruk et. Al, 2014), (Cohen et. al, 2014) and (Philipps et. Al, 2015). Only the most relevant features of the hydrofoil are reported below.

The isotropic and composite hydrofoils have an identical geometry consisting of a trapezoidal planform with a 300 mm span, and a varying chord in the spanwise direction (Figure 1 and Figure 2). The basechord is 120 mm and the tipchord is 60 mm. The section is a NACA0009 with a modified thicker trailing edge to allow the manufacture of the hydrofoils. To clamp the hydrofoil on the water tunnel wall, the root of the hydrofoil is prolonged with a 20 mm metallic plate, pictured in blue on Figure 2, (A). Two additional metallic plates are used to hold both sides of the hydrofoil in a mounting flange, and a fairing disk is then added to pinch the plates (refer to Figure 1). The incidence of the hydrofoil within the water tunnel can still be varied using this arrangement, and the effective wet span in still 300 mm.

The isotropic hydrofoil was made of aluminum, while the composite one consists of a hybrid design shown in Figure 2 (B). First a thick sandwich glass mat fabric was used at mid-chord to help resin distribution during the RTM (Resin Transfert Molding) process. Then, several plies consisting of unidirectional carbon fiber fabric and biaxial E-glass were stacked on the mat for structural properties. Last, a basket weave E-glass fabric was used

as the outer ply to aid surface quality. Since the thickness and the chord are not constant along the span, some plies need to be progressively reduced and dropped relative to the initial stacking sequence shown on Figure 2 (B). This is done similarly to the layers of an onion: the central mat fabric is kept constant along the span, as well as the basket weave E-glass outer ply, and the internal plies the closest to the center are dropped. All fibers are oriented along their longitudinal direction, i.e the 0°-axis. Table 1 sums up the mechanical properties of the different plies for the composite hydrofoil. The two hydrofoils tested in the present study corresponds to the Type II-AL (aluminum) and Type II-CFRP00 (composite with 0° fiber orientation) hydrofoils, see (Zarruk et. Al, 2014) for more details.

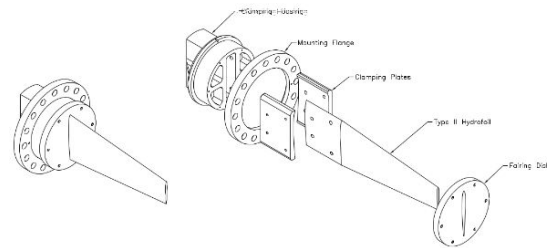


Figure 1. Schematic illustration of the general mounting arrangement of the hydrofoil for water tunnel tests, from (Cohen et. al, 2014)

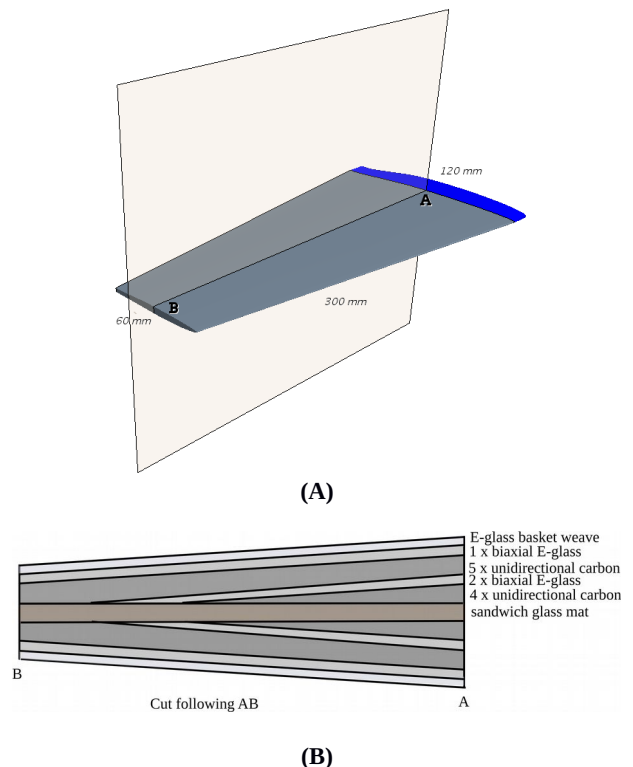


Figure 2. (A) Geometry of the hydrofoil in dark gray, with its clamping disk in blue and (B) layers arrangement of the composite hydrofoil featuring the plies drops - cut following the mid-plane section from (A).

Table 1. Properties of the Composite Plies

	Carbon	E-glass	Basket	Mat
ρ [g/cm ³]	1.55	1.78	1.69	7.40
E_{11} [Mpa]	118000	20600	15000	3000
E_{22} [MPa]	6500	20600	15000	5000
ν_{12}	0.27	0.32	0.13	0.26
G_{12} [MPa]	4500	4000	4000	2500
G_{23} [MPa]	4500	4000	4000	2500
G_{13} [MPa]	3300	3300	3300	3300
Orientation [°]	0	0	0	isotropic

3 NUMERICAL METHODS

In this section we introduce the governing equations for the fluid-structure problem and the coupling between the two physics, along with the numerical methods used. The numerical set-up is then detailed.

3.1 Governing Equations

In this problem we consider a structure Ω surrounded by a fluid Ω_f with an interface Γ , Figure 3. The fluid is characterized by its velocity field $\mathbf{v}(x,t)$ and pressure p , and the solid by its displacement field $\mathbf{u}(x,t)$, deformation field $\epsilon(x,t)$ and stress field $\sigma(x,t)$.

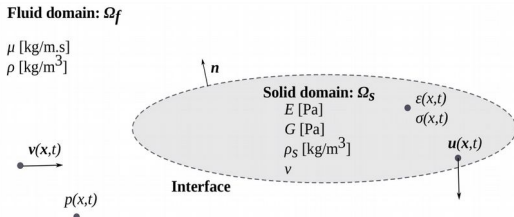


Figure 3. Theoretical formulation of the fluid-structure interaction problem.

3.1.1 Governing Equations for the Fluid

The fluid is modeled using *Reynolds-Averaged Navier-Stokes* equations (RANS), where the incompressible Navier Stokes equations can be written as (1), with V the local velocity and P the pressure.

$$\frac{\partial V_i}{\partial x_j} = 0$$

$$\rho \left(\frac{\partial \bar{V}_i}{\partial t} + \frac{\partial \bar{V}_i}{\partial x_j} \bar{V}_j \right) = \rho f_i - \frac{\partial \bar{P}}{\partial x_i} + \nu \frac{\partial^2 \bar{V}_i}{\partial x_i \partial x_j} \quad (1)$$

3.1.2 Governing Equations for the Structure

The structure behavior is governed by the fundamental law of the dynamics, the displacement-deformations relation (valid in the case of small deformations), and in the case of composite structures, the anisotropic law of elasticity. These equations are written as (2), with C the *stiffness matrix*, consisting of 21 independent coefficients.

$$\rho_s \frac{\partial u_i^2}{\partial t^2} - \frac{\partial \sigma_{ij}}{\partial x_j} = \rho_s g_i$$

$$\epsilon_{ij} = \frac{1}{2} \left(\frac{\partial u_i}{\partial x_j} + \frac{\partial u_j}{\partial x_i} \right) \quad (2)$$

$$\bar{\epsilon} = C \bar{\sigma}$$

3.1.3 Coupling Equations

Two types of coupling equations (3) are considered: A kinematic condition enforcing the continuity of the velocities in the fluid and in the solid at their interface, and a dynamic condition for the force balance at the interface.

$$v_i = \frac{\partial u_i}{\partial t}$$

$$\sigma_{ij} \cdot n_j = \left(-p \delta_{ij} + \mu \left(\frac{\partial v_i}{\partial x_j} + \frac{\partial v_j}{\partial x_i} \right) \right) \cdot n_j \quad (3)$$

3.2 Numerical Set-up and Boundary Conditions

This part describes the fluid and structure models, along with the coupling parameters chosen for the simulations. The same fluid model can be used both for the isotropic and composite hydrofoils, however, two different structure models have to be set-up.

3.2.1 Fluid Numerical Model

The fluid flow is obtained using the commercial Finite Volume CFD software Starccm+, based on 3D RANS equations. The fluid domain have the same square section and dimensions than the experimental water tunnel (0.6 m high and 2.6 m long). The incoming flow is considered uniform with a reference velocity U . A symmetry condition ($\mathbf{v} \cdot \mathbf{n} = 0$) is imposed on the water tunnel walls, whereas a no slip condition ($\mathbf{v} \cdot \mathbf{t} = 0$) is set at the hydrofoil's surface (refer to Figure 4). The later can be modified due to the displacements imposed from the structure code. The numerical clamping is done by locating the base of the hydrofoil on one of the water tunnel wall. The *SST k- ω* turbulence model (Menter, 1994) is used in the simulation to accurately predict the boundary layer detachment along the hydrofoil.

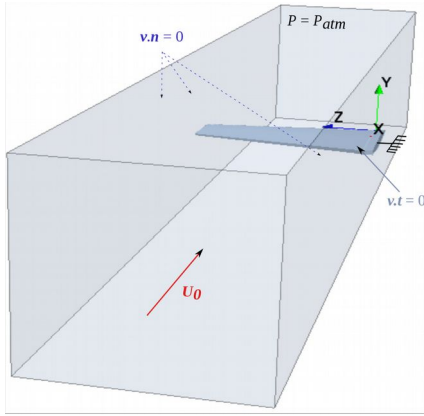


Figure 4. Schematic illustration of the fluid domain and boundary conditions.

The domain is discretized using polyhedral elements, with a structured mesh close to the wall to capture the boundary layer. It is particularly refined at the leading and trailing edges in the near wall region and in the wake. An illustration of the mesh is presented on Figure 5 for a section located at the root of the hydrofoil. The boundary layer mesh was performed in order to satisfy a Log Law representation, *i.e.* $50 < y^+ < 70$ using a structured grid in the wall vicinity, see Figure 5. Unsteady simulations are considered using a second order backward Euler scheme. The time step is set to satisfy $CFL = U \Delta t / \Delta x \leq 1$, where Δx is the mean cell size in the chordwise direction at the hydrofoil's surface.

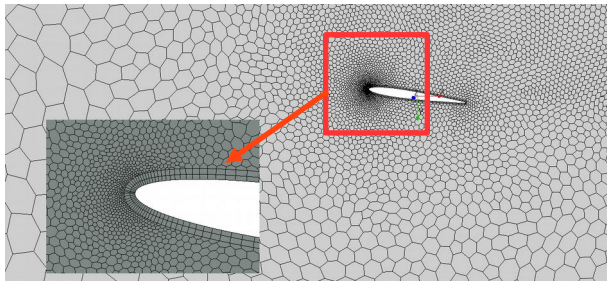


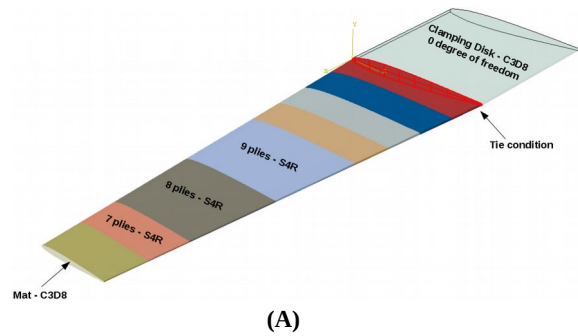
Figure 5. Illustrations of the fluid domain mesh

3.2.2 Structure Numerical Model

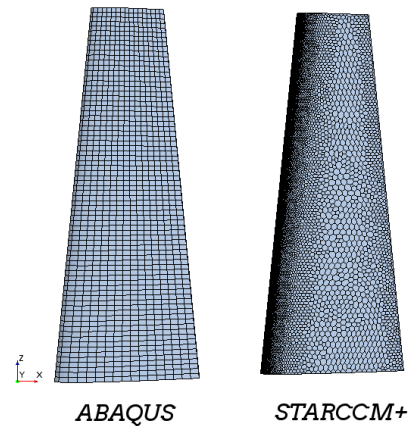
The structure model is setup both for the isotropic and composite hydrofoils. The Finite Element Method is used with an explicit scheme to solve the anisotropic equations and the fundamental relation of the dynamic for the displacements, stresses and deformations fields. Indeed, the time step is identical for the fluid and solid solvers, and is small enough to enable the use of an explicit solver for the structure. This leads to a faster resolution of the structure equations.

To account for the clamping disk, the geometry is extended by 20 mm at the base of the hydrofoil (see Figures 1 and 2A), and all the nodes on this additional part are restrained along all directions. The clamping disk is then defined as stainless steel, and solid continuum elements (C3D8) are chosen for the 3D mesh. The

numerical model is common between the isotropic and composite hydrofoils, and differs when defining the material properties and the mesh of the hydrofoil. The isotropic hydrofoil is fully modeled with aluminum, and solid continuum C3D8 elements are used for the mesh. For the composite hydrofoil, these elements cannot account for the stacking sequence of plies described previously and illustrated on Figure 2 (B). Thus the inner and central part of the hydrofoil corresponding to the isotropic sandwich glass mat is modeled classically, using C3D8 solid continuum elements, and a skin with S4R shell elements is added on top and below it (see Figure 6A). The plies are described in the shell elements properties, reported in Table 1. Moreover, as the thickness varies along the span, so does the number of plies: One then needs to cut the hydrofoil into sections, each one of them with a specific number of plies. Figure 6 (A) shows the different sections used to account for the variable number of plies. Figure 6 (B) shows a comparison between the fluid and structure meshes on the hydrofoil surface.



(A)



(B)

Figure 6. (A) Model of the composite hydrofoil showing the different sections used to account for the variable number of plies within the hydrofoil, and the mesh elements types, (B) Fluid and structure meshes on the hydrofoil

3.3 Coupling Methodology

In the fluid-structure coupled computation, data is transferred from the fluid to the structure solver to model the exchange of energy between the two physical domains, see Figure 7 (A). In this work, the coupling is realized using the Co-simulation Director Engine (CSE)

already implemented in Abaqus to interact with third-party codes such as Starccm+, see Figure 7 (B).

Two types of calculation are performed, based on different coupling algorithms. A non coupled procedure is first set. It uses only one converged fluid solution, then exports the pressure field to get the structure solution. Tightly coupled fluid structure computations are also performed. They are based on a two way coupling between the fluid and structure codes, where staggered iterations within one coupling time step help for the energy conservation at the interface, as illustrated on Figure 7 (C). To advance in time, the displacements and pressure must indeed reach a state of convergence between the values $(u,p)^k$ and $(u,p)^{k+1}$, or be forced to move forward in time t_i after ten exchanges, where k corresponds to the sub-iteration number. Moreover, the fluid resolution scheme is implicit, so for each data exchange, the pressure p_i^k is determined using several fluid internal iterations to reach convergence.

To increase the stability of the coupled calculation, the displacement solution imported in the fluid solver is under-relaxed to progressively implement the current value during the coupling time. The first two data exchanges are not under-relaxed, then the relaxation factor is optimally adjusted between 0.2 and 0.5.

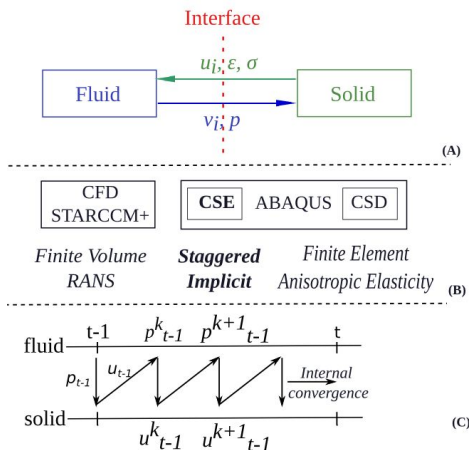


Figure 7. (A) Principle of a fluid-structure coupling, (B) Numerical Codes and Methods used in this work, (C) Details of the Staggered Implicit Coupling Algorithm

4 RESULTS

This part details the results of the different simulations, including the validation of the fluid and structure models separately, and the results from non coupled and coupled simulations.

4.1 Fluid Model Validation

The fluid model is first checked for the case of infinitely rigid hydrofoil (no coupling).

4.1.1 Mesh Convergence Study

A mesh convergence study on the fluid domain is performed for 8° angle of attack. Seven meshes are considered, with numbers of elements ranging from

217,810 to 4,004,628, where the mesh topology and boundary layer mesh is kept, see section 4.1 and Table 2. The convergence of hydrodynamic coefficients are presented on Figure 8. It shows that the solution is converged for the lift coefficient starting from 543,535 elements.

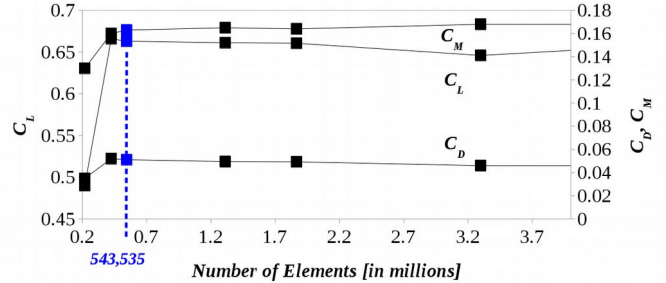


Figure 8. Mesh convergence study using seven meshes for the configuration with 8° angle of attack and $Re = 600,000$

Table 2. Size of the mesh elements for the seven meshes used in the convergence study, in % of the mean chord (90 mm)

Number of elements	Wake	Hydrofoil	Leading Edge
217,810	1	0.67	0.07
423,556	0.83	0.57	0.03
543,535	0.73	0.4	0.027
1,311,230	0.47	0.4	0.02
1,865,994	0.4	0.4	0.02
3,298,329	0.33	0.33	0.013
4,004,628	0.3	0.27	0.013

4.1.2 Hydrodynamic Coefficients Prediction

Next, comparisons between the present computations and experimental measurements of Zarruk et al. 2014 on the hydrodynamic coefficients are carried out for angles of attack ranging from 0° to 14° . Results are first presented on Figure 9 (A). The results match very well when the flow is attached ($0 < \alpha < 8^\circ$), whereas the computations underestimate the drag after stall occurs. Figure 9 (B) shows the performance curve relative to the angle of incidence, where the over prediction of the drag lead to lower performances for the computations as compared to the experiments of Zarruk et al. 2014.

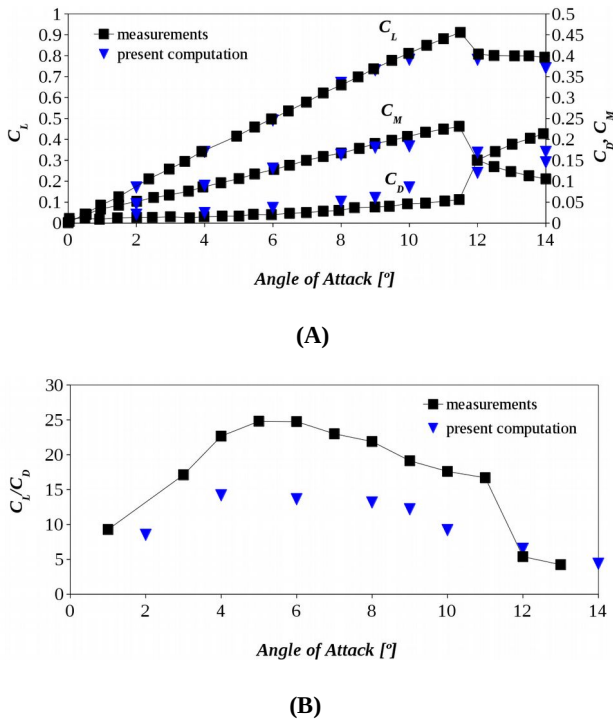


Figure 9. (A) Comparisons between numerical computation and experimental measurements of Zarruk et al. 2014, on hydrodynamic coefficients for angles of incidence ranging from 0° to 14°, (B) performances curve. $Re=600,000$

4.2 Structure Model Validation

The validation of the structure model requires an iterative approach. First, the weight of the hydrofoil is numerically adjusted to match the experimental weight by tuning the density coefficient of the materials. Then, a convergence study is carried out on the mesh, for the three first modes of the hydrofoil. For this purpose, material properties are set *a priori* to the experimental values determined in (Zarruk et al, 2014), (Cohen et. al, 2014) and (Philipps et. Al, 2015). The first converged mesh is selected, and natural bending and twisting frequencies are adjusted using Young's Modulus E_{11} and E_{22} and the Shear Modulus G of the structural materials (unidirectional carbon and¹² E-glass weave). until the numerical frequencies match the experimental ones. A new mesh convergence study is then realized using the adjusted material properties, and so on.

The mesh convergence study for the first three modes of the aluminum hydrofoil is presented Figure 10. The two first modes are bending modes (Figure 11 (A) and (B)), and the third mode is a torsion mode (Figure 11 (C)). Meshes tested are the following, using the notation [total number of elements for the wet part of the hydrofoil, elements across the thickness]: [704, 1], [1 980, 2], [6 804, 3], and [28 050, 4]. The mesh of 1 980 elements C3D8R is chosen for the aluminum hydrofoil, even if not totally converged, for schedule reasons. A mesh of 5 800 elements is used for the composite hydrofoil (2 400 C3D8R + 2 400 S4R). Concerning the material properties, in the case of the aluminum hydrofoil, the experimental Young's Modulus is 71 Gpa, and a value of 80 Gpa is used

in the numerical model. For the composite hydrofoil, the properties used in the numerical model are presented in Table 1, and are to be compared with the experimental data from (Zarruk et al, 2014), (Cohen et. al, 2014) and (Philipps et. Al, 2015). Table 3 presents such a comparison and shows that the numerical properties are relatively close to the experimental ones. The discrepancies are due to the use of non-fully converged mesh: Indeed, from Figure 10 one can observe that the frequencies are increasing with the number of elements, and are actually higher than the experimental values for the converged mesh. As a consequence, using a fully converged mesh to adjust the material properties imply reducing the numerical stiffness of the structure, and getting even closer to the experimental material properties . This work is undergoing. For the isotropic hydrofoil, only experimental natural bending frequency is provided, and numerically matched. For the composite hydrofoil, the validation of the numerical material properties is presented in Table 4.

Table 3. Adjustments of the structural properties of Carbon and E-glass plies to validate the structure model by matching the numerical and experimental frequencies for the composite hydrofoil

[GPa]	Carbon expe	Carbon num	E-glass expe	E-glass num
E_{11}	15.3	11.8	15.1	20.6
E	12.8	6.5	19.3	20.6
G^{22}	3	4.5	4.2	4
12				

Table 4. Summary of structure model validation

	Weight [g]	Bending Mode [Hz]	Twisting Mode [Hz]
Al - expe	-	100	-
Al - numerical	-	100.5	-
Experimental Composite	409.6	112	415
Composite Hydrofoil	408	107	418

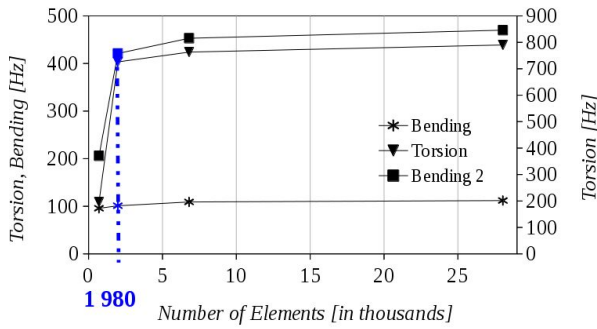


Figure 10. Structural Mesh Convergence Study on the First Three Modes

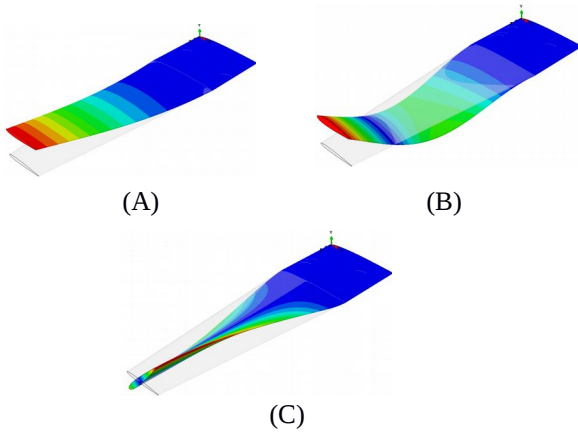


Figure 11. Frequency analysis of the aluminum hydrofoil (A) First bending mode, (B) Second bending mode and (C) First torsion mode

4.3 Non coupled and Coupled Results

This section presents results obtained for the non coupled and coupled calculations for an angle of attack of 8° . Results of the non coupled calculation are first used to validate the accuracy of the pressure transfer between the fluid and solid solvers, using a Least Squares interpolation method. Figure 12 shows the pressure computed with the CFD code and the mapped pressure read in the CSD code, relative to the fluid and structure meshes shown on Figure 6 (B). It is shown that the pressure gradient at the hydrofoil's surface is correctly interpolated in CSD code, whereas the mesh topology is quite different.

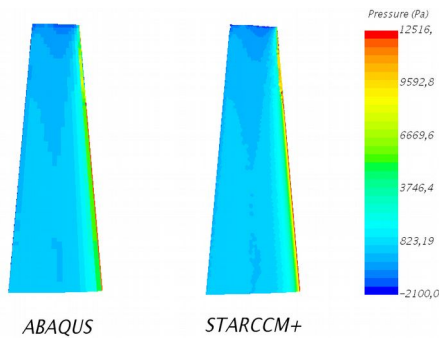
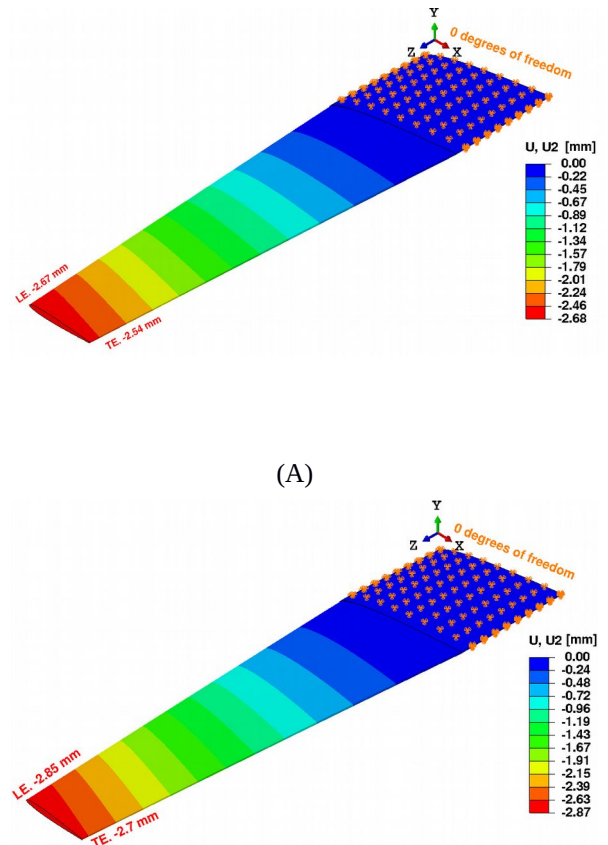


Figure 12. Validation of the transfer of pressure between the fluid solver and the structure solver, $\alpha=8^\circ$

The maximum tip displacement of the hydrofoil under hydrodynamic loading is then determined for the non coupled and the coupled calculations, and compared against experimental measurements. Results are reported in Table 5 for the isotropic hydrofoil, and in Table 6 for the composite hydrofoil. Figure 13 also presents the deformation of the hydrofoils. There is a general good agreement between the present computations and measurements. For the aluminum hydrofoil, the computed drag coefficient is above the experimental value. There is also an under prediction of the tip displacement, that is greater for the non-coupled computation. Even though the twist is very low, it is clear that accounting for the fluid-structure interaction, *i.e* the coupling between twist deformation and lift coefficient, increases the accuracy of the computation.

For the composite hydrofoil, the tip displacement is on the contrary slightly over predicted both at the leading and trailing edges. Moreover, the interaction between the hydrofoil's twist and the lift force is enhanced as compared to the aluminum hydrofoil, due to the higher flexibility. This results in an increase of lift force, bending and twist deformations and tip displacement... The natural frequencies of the composite hydrofoil are greater than the experimental ones as compared to the aluminum hydrofoil. It means that the flexibility is reduced relative to the experiments. This could explain the higher discrepancy between the simulation and the measurement for the composite hydrofoil.



(B)

Figure 13. (A) Displacements along the Y-direction for the aluminum hydrofoil and (B) for the composite hydrofoil, $\alpha=8^\circ$. LE = Leading Edge and TE = Trailing Edge

Table 5. Results of the fluid-structure computation on the aluminum hydrofoil. Results for the displacements are provided for the Leading Edge and Trailing Edge, $\alpha=8^\circ$

Aluminum hydrofoil	C_L	C_D	Max. tip Disp.[mm]	Twist [deg]
Measurements	0.50	0.020	2.1	-
Non coupled computation	0.49	0.033	1.92	-0.025
Coupled computation	0.50	0.033	1.98	-0.029

Table 6. Results of the fluid-structure computation on the composite hydrofoil. Results for the displacements are provided for the Leading Edge and Trailing Edge, $\alpha=8^\circ$

Composite hydrofoil	C_L	C_D	Max. tip Disp.[mm]		Twist [deg]
			LE	TE	
Measurements	0.51	0.026	2.6	2.5	0.09
Non coupled computation	0.49	0.033	2.67	2.54	0.13
Coupled computation	0.5	0.033	2.85	2.7	0.15

5 CONCLUSION AND FURTHER WORK

In this work, the flow over flexible NACA009 3D hydrofoils is simulated using a finite volume/finite element coupling between the CFD solver Starccm+ and the CSD solver Abaqus. Two hydrofoils of the same dimensions and trapezoidal planform geometry, but of different materials, were simulated in a cantilevered arrangement to assess their hydroelastic behavior, and results were compared with experiments from Zarruk et al. 2014. The first hydrofoil was made of aluminum, and the second of carbon-fiber reinforced plastic (CFRP) with fibers oriented at 0° . Fluid models and structure models were setup, preliminary validated, and then computed using non coupled and coupled procedures. The results were validated on the lift and drag coefficients, and the maximum tip displacement of the hydrofoil. It shows overall very good agreement with the reference study. Moreover, the numerical study confirmed that the composite hydrofoil has a higher twist deformation than the aluminum hydrofoil, due to the 0° fiber orientation along the span, and is more flexible. Natural bending and twisting frequencies are adjusted using Young's Modulus E and the Shear Modulus G of the structural materials, and are greater than that of the experiments, explaining the reduced stiffness of the composite hydrofoil.

Moreover, the larger twist deformation will tend to amplify the coupling effect induced by the local increase of the angle of attack along the span, which interacts with the lift force.

In the near future, unsteady fluid structure coupling will be carry out on the hydrofoil to analyze the behavior of composite hydrofoils under stall conditions. This work will help for the design of a newly developed composite marine propeller.

Acknowledgements

The authors thanks DCNS for its financial support through a collaborative grant DCNS-LHEEA. The calculations were performed on a Nehalem cluster at CRIANN, France.

REFERENCES

- Blasques, J-P, Berggreen, C., Andersen, P. (2010). 'Hydroelastic Analysis and Optimization of a Composite Marine Propeller'. *Marine Structures* **51**, pp.22-38
- Cohen, B., Dylejko, P., Moore, S., & Philipps, A. (2014). 'Numerical Modelling and Experimental Determination of the Dynamic Behaviour of Composite Structures'. *Inter-noise 2014* Melbourne, Australia
- Chen, B., Neely, S., Michael, T., Gowing, S., Szwere, R., Buchler, D., Schult, R. (2006). 'Design, Fabrication and Testing of Pitch-Adapting (Flexible) Composite Propellers'. *The SNAME Propellers/Shafting Symposium* Williamsberg
- Garg, N., Kenway, G. K., Martins, J., Young, Y. L. (2017). 'High-Fidelity Multipoint Hydrostructural Optimization of a 3-D Hydrofoil.' *Journal of Fluid and Structures* **71**, 15-39.
- Garg, N., Kenway, G. K., Lyu, Z., Martins, J. R., Young, Y. L. (2015). 'High-Fidelity Hydrodynamic Shape Optimization of a 3-D Hydrofoil.' *Journal of Ship Research*, **59**(4), 209-226.
- He, X.D., Hong, Y., Wang, R.G. (2012). 'Hydroelastic Optimization of a Composite Marine Propeller in a Non-Uniform Wake'. *Ocean Engineering* **39**, pp.14-23
- Lee, Y-J, Lin, C-C. (2004). 'Optimized Design of Composite Propeller'. *Mechanics of Advanced Materials and Structures* **11**, pp.17-30
- Liu, Z., Young, Y.L.. (2007). 'Utilization of Deformation Coupling in Self-Twisting Composite Propellers'. *16th International Conference on Composite Materials* Kyoto, Japan
- Liu, Z., Young, Y.L.. (2009). 'Utilization of Bend-Twist Coupling for Performance Enhancement of Composite Marine Propellers'. *Journal of Fluid and Structures* **25**, pp.1102-1116

- Phillips, A., Nanayakkara, A., Cairns, R., St John, N., Herath, M. T., Zarruk, G. A., & Brandner, P. A. (2015). 'Effect of Material Anisotropy on the Structural Response of Flexible Composite Hydrofoils'. SAMPE Conference Proceedings Baltimore, Maryland
- Plucinski, M.M., Young, Y.L., Liu, Z. (2007). 'Optimization of a Self-Twisting Composite Marine Propeller using a Genetic Algorithms'. 16th International Conference on Composite Materials Kyoto, Japan
- Yamatogi, T., Murayama, H., Uzawa, K., Kageyama, K., & Watanabe, N. (2009). 'Study on Cavitation Erosion of Composite Materials for Marine Propeller'. 17th International Conference on Composite Materials Edinburgh, Scotland.
- Young, Y. L., Motley, M., Barber, R., Chae, E. J., & Garg, N. (2016). 'Adaptive Composite Marine Propulsors and Turbines: Progress and Challenges'. Applied Mechanics Reviews
- Zarruk, G. A., Brandner, P. A., Pearce, B. W., & Phillips, A. W. (2014). 'Experimental study of the steady fluid-structure interaction of flexible hydrofoils'. Journal of Fluids and Structures **51**, pp.326-343